Probing the electrical anisotropy of multilayer graphene on the Si face of 6*H*-SiC

B. Jouault,[1,2] B. Jabakhanji,[1] N. Camara,[3] W. Desrat,[1] A. Tiberj,[1] J.-R. Huntzinger,[1] C. Consejo,[1] A. Caboni,[3] P. Godignon,[3] Y. Kopelevich,[2,4] and J. Camassel[1,2]

[1]*Groupe d'Étude des Semiconducteurs, Université Montpellier 2, cc074, pl. Eugène Bataillon, 34095 Montpellier Cedex 5, France*

[2]*CNRS, UMR 5650, cc074, pl. Eugène Bataillon, 34095 Montpellier Cedex 5, France*

[3]*CNM, Campus UAB, Bellaterra (Barcelona), Spain*

[4]*Instituto de Física Gleb Wataghin, Universidade Estadual de Campinas, Unicamp 13083-970 Campinas, SP, Brazil*

(Received 27 April 2010; revised manuscript received 19 July 2010; published 24 August 2010)

We studied the in-plane magnetoresistance $R(B,T)$ anisotropy in epitaxial multilayer graphene films grown on the Si face of a 6*H*-SiC substrate that originates from steplike morphology of the SiC substrate. To enhance the anisotropy, a combination of argon atmosphere with graphite capping was used during the film growth. The obtained micro-Raman spectra demonstrated a complex multilayer graphene structure with the smaller film thickness on terraces as compared to the step edges. Several Hall bars with different current/steps mutual orientations have been measured. A clear anisotropy in the magnetoresistance has been observed, and attributed to variations in electron mobility governed by the steplike structure. Our data also revealed that (i) the graphene-layer stacking is mostly Bernal type, (ii) the carriers are massive, and (iii) the carriers are confined to the first 2–4 graphene layers following the buffer layer.

DOI: 10.1103/PhysRevB.82.085438 PACS number(s): 72.80.Vp, 78.67.Wj

I. INTRODUCTION

The graphitization of SiC surfaces is a promising technique to design large area graphene-based devices, such as, e.g., sensors or Hall bars (HBs) for quantum metrology.[1] To this end, both Si and C faces of SiC substrates can be considered as a starting material.[2–5] On the one hand, due to recent developments such as the growth of few-layer graphene (FLG) under an argon atmosphere, the growth of FLG on the Si face appears promising. FLGs have been grown in this way on large dimensional wafers, with mobility high enough to observe quantum Hall effects.[6] On the other hand, on the C face, long uniform graphene ribbons have been grown[7] but they remain electrically isolated and the formation of a uniform coverage on the substrate with a homogeneous FLG remains challenging.

Whatever the growth technique, a common belief is that for a complete graphene coverage, epitaxial graphene exhibits isotropic transport properties. In other words, one should not expect any effect of the underlying surface structure, and the FLG should behave like a uniform carpet in the directions parallel and perpendicular to the substrate steps that usually form during the growth.

In this work, we have checked this hypothesis by enhancing the structural anisotropy. We have used a combination of argon atmosphere with graphite capping technique and found the following. First, there is electrical anisotropy of the transport properties. Second, this anisotropy originates from the enhanced scattering rate at the step edges, and not from a discontinuity of the graphene film. This conclusion agrees with the fact that the FLG coverage is continuous over the substrate, although the film thickness is not spatially uniform.

II. FLG GROWTH

We used a 1×1 cm^2 substrate, cutted from the (0001) Si-terminated 6*H*-SiC wafer. To increase the FLG anisotropy, a modified growth procedure was used with respect to the one detailed in our previous work.[7] After cleaning the substrate in the usual way, the growth was performed under argon[4,6] at atmospheric pressure, at 1750 °C for 20 min, with a graphite cap covering the sample. The resulting morphology, observed by atomic force microscope (AFM), is shown in Fig. 1. From this AFM scan, a pronounced steplike morphology of the SiC substrate is evident. The average terrace width is 5 μm, and the steps have an average height of 10 nm. Additionally, the optical microscope sample characterization revealed a remarkable homogeneity of width and orientation of the terraces on a large scale of 1 cm^2. It also revealed the existence of thicker FLG stripes close to the step edges.

III. OPTICAL AND RAMAN ANALYSIS

In Fig. 2(a), we show an optical image collected in the reflection mode on a 40×30 μm^2 sample area. The dark areas correspond to central parts of terraces. The light gray regions correspond to thicker stripes near the edges, on which the incident light reflects more. In what follows, for sake of simplicity, we call the thick graphene regions "stripes" and the thin graphene regions "terraces."

In Fig. 2(b), we show a micro-Raman map collected on the same area as shown in Fig. 2(a). The color of the map corresponds to the integrated intensities of the G band and

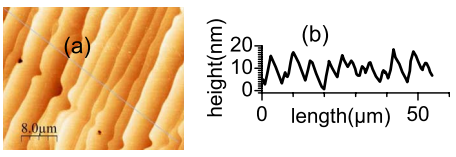

FIG. 1. (Color online) (a) AFM color map of the FLG sample. Notice the large step bunching, with an average step height of 10 nm. The gray line corresponds to the AFM profile shown in (b).

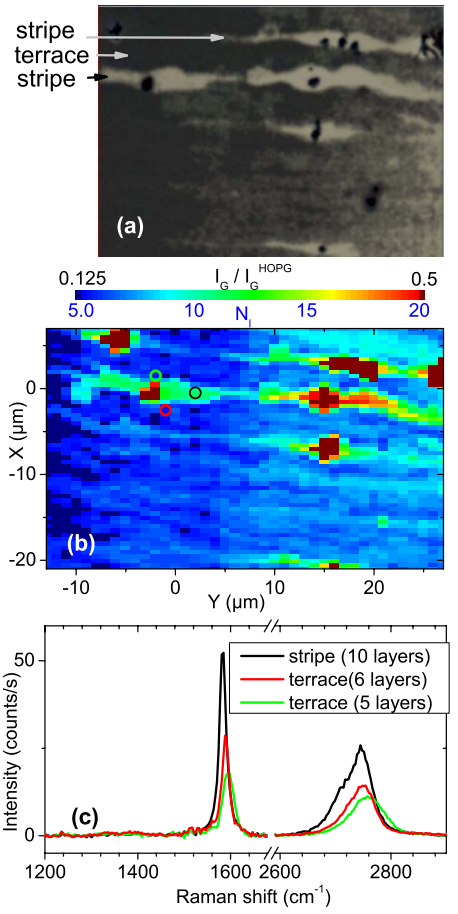

FIG. 2. (Color online) (a) Optical image of the graphene surface and (b) corresponding Raman cartography. The color gives the intensity of the integrated G band, normalized by a reference (the intensity of the G band of a HOPG). N_l is an estimation of the number of layers. The stripes at the edges of the terraces indicate a thicker graphite in these regions. The intense red spots correspond to carbon pits induced during the growth by stacking faults. Excluding the red spots, the Raman intensity corresponds to 3–11 monolayers. (c) The asymmetry in the profile of the 2D band reveals a coupling between the graphene planes. The green, red, and dark spectra have been obtained from the positions indicated by green, red, and dark circles in (b), respectively.

becomes more intense (red) at the edges of terraces. This is also the case for the integrated intensity of the two-dimensional (2D) band. Therefore, the FLG stripes noticed by optics are significantly thicker. From the normalized intensity of the G band,[7] we extracted the mean thickness and found about five layers in the center of terraces [blue areas in Fig. 2(b)] and about 11 layers in the stripes (green areas). The red spots are the carbon-rich graphite pits observed in optics, induced by an increased growth rate due to the presence of defects such as dislocations or stacking faults.

Three Raman spectra collected on terraces and on a stripe are plotted in Fig. 2(c) in green, red, and black, respectively. The Raman bands are shifted toward higher frequencies, due to the differential dilatation between the FLG and the substrate during the cooling down of the sample after growth. Thicker regions are less shifted, indicating a partial relaxation of the strain. The thickest FLG possesses most of

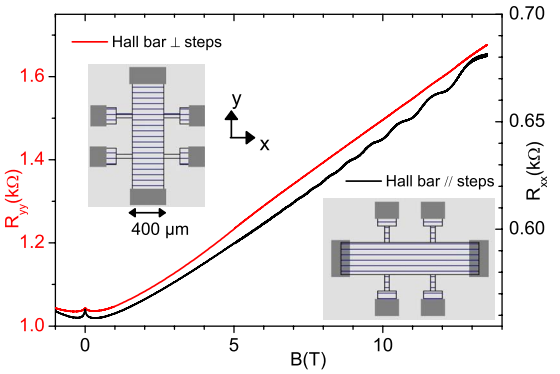

FIG. 3. (Color online) Magnetoresistance of two large Hall bars, respectively: perpendicular (R_{yy}, red line) and parallel (R_{xx}, black line) to the steps. The magnetic field ranges from −1 to 12.5 T.

graphene layers well relaxed, such that the shape of the 2D peak is similar to the shape of the 2D peak of graphite, demonstrating a characteristic lower frequency shoulder.[8] Therefore, for stripes at the edges, the asymmetry of the 2D peak in Fig. 2(c) is a clear indication of Bernal stacking. The asymmetry persists but is strongly reduced on the terraces, see Fig. 2(c), red and green curves. It has already been observed that even without strain, the low-frequency shoulder of FLGs becomes usually less visible when the number of layers decreases.[9,10] Moreover, an additional blurring of the 2D peak shape can occur for thin FLGs whose thickness is comparable to the strain relaxation length. Taking all these together, we conclude that the graphene-layer stacking at terraces is also Bernal type, being consistent with the results reported in Ref. 11 and transport measurements performed in the present work.

IV. TRANSPORT EXPERIMENTS

To verify effect of the sample structural anisotropy on the electrical transport, we measured standard Hall bars as shown in Fig. 3. The Hall bars were prepared by means of optical lithography combined with oxygen plasma etching. The typical sample length is 1.5 mm and the distance between adjacent lateral probes $L=500$ μm. The samples of widths $W=100$, 175, and 400 μm were used for measurements. For each W, two similar HBs with orientations parallel and perpendicular to the steps have been prepared. In the following, we define x as the axis parallel to the stripes. The resistance $R_{xx}(T,B)$ and $R_{yy}(T,B)$ measurements performed on Hall bars with different current/steps mutual orientation, demonstrated a sizable anisotropy. This is shown in Fig. 3, where we depict the longitudinal resistances measured at 4.2 K for the two large Hall bars, with a magnetic field applied perpendicularly to the sample main plane.

At room temperature, this anisotropy persists but is reduced by 20%. Such results, obtained for all pairs of Hall bars, cannot be attributed to resistance variations from one bar to another.

In addition, Shubnikov de Haas (SdH) oscillations, observed for both R_{xx} and R_{yy}, see Fig. 3, are also sensitive to the anisotropy. As can be seen from Fig. 3, SdH oscillations

are clearly visible in $R_{xx}(B)$ but they are strongly damped in $R_{yy}(B)$, and can be seen only after subtraction of a large magnetoresistance monotonic background signal. In contrast, the Hall voltage does not depend on the orientation of the Hall bar and is roughly linear in B up to 13 T. We conclude then that the electron density $n_s=10^{13}$ cm^{-2} is uniform and has a little variation between 4 and 300 K. Hence, one concludes that terraces and thicker stripes have different mobilities. In the Hall bars where the current flows parallel to terraces, the low mobility regions can be avoided and the SdH oscillations reveal themselves. However, in the Hall bars with a current flowing perpendicular to the terraces, the current cannot avoid the low mobility regions, and the SdH oscillations are strongly suppressed.

Starting from this assumption, we now determine which area (terrace or stripe) corresponds to the highest mobility. We model the resistances R_{xx} and R_{yy} either as a sum of conductances if the current flows parallel to the stripes or a sum of resistances, if the current flows perpendicularly,

$$\frac{\alpha}{R_{xx}} = \lambda/\rho_s + (1-\lambda)/\rho_t, \quad \frac{R_{yy}}{\alpha} = \lambda\rho_s + (1-\lambda)\rho_t, \qquad (1)$$

where ρ_t and ρ_s are the sheet densities of the terraces and the stripes, respectively, $\alpha=L/W$ is the geometric factor of the Hall bar, $\lambda=w_s/(w_t+w_s)$ depends on the width of the stripes w_s, and the width of the terraces w_t. On average, from optical and Raman analysis, w_s is estimated to be ten times smaller than w_t and we get $\lambda\approx 0.1$.

Solving these equations leads to a quadratic equation with two different solutions for ρ_t and ρ_s. We first examine the solution corresponding to the stripes being less resistive than the terraces: $\rho_s<\rho_t$. From Fig. 3(a) which corresponds to Hall bars with $\alpha=1.25$, we get $\rho_s\approx 80\ \Omega$ and $\rho_t=900\ \Omega$ at 4 K. From $1/\rho=n_s e\mu$, we obtain mobilities $\mu_t \approx 700$ cm^2/V s and $\mu_s\approx 8000$ cm^2/V s. This μ_s value being larger than what is commonly reported for similar samples at high electron density, we discarded this solution. Coming to the second possibility (the stripes being more resistive than the terraces: $\rho_s>\rho_t$) we get $\rho_s\approx 4500\ \Omega$ and $\rho_t=400\ \Omega$ at 4 K or, equivalently, $\mu_s\approx 150$ cm^2/V s and $\mu_t\approx 1500$ cm^2/V s. These values appear more comparable to the literature.

Next, we turn our attention to the magnetoconductance peak observed at low magnetic fields (0–1 T) and presented in Figs. 4 and 5. In principle, this peak can be accounted for by the weak localization (WL) (Ref. 12): (i) it is not observed when the magnetic field is applied in the sample's plane; (ii) the peak height varies roughly as $\ln(T)$ with slope $\pi h/e^2$, see Fig. 4(a); (iii) the amplitude of the peak is on the order of $e^2/\pi h$ at $T\approx 4$ K and decreases when T increases, disappearing around $T=30$ K. However, the WL peak has different heights and shapes for R_{xx} and R_{yy}. This is because the standard theory of weak localization assumes a homogeneous film and cannot be applied straightforward to our anisotropic samples. The conductivities of, both, terraces and stripes at low magnetic field have to be extracted first from Eq. (1). The results are shown in Fig. 5. The WL peak almost disappears in the conductivity attributed to the stripes (red squares) but remains large in the conductivity attributed to the terraces (black squares). This is a clear indication that the WL-type peak originates from the high mobility part of FLGs (terraces).

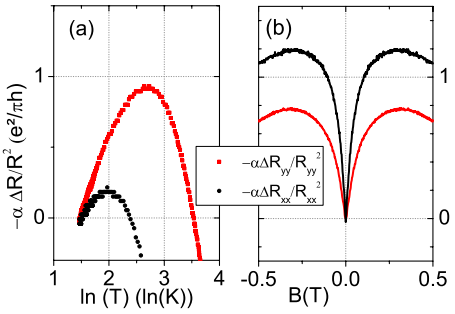

FIG. 4. (Color online) (a) Variations in the longitudinal conductance versus temperature collected for two similar Hall bars, respectively: perpendicular ($-\alpha\Delta R_{yy}/R_{yy}^2$, red line) and parallel ($-\alpha\Delta R_{xx}/R_{xx}^2$, black line) to the FLG steps. The conductance shows a logarithmic dependence on T below 30 K. (b) magnetoconductances collected at low magnetic fields between −0.5 and +0.5 T.

To describe the magnetic field dependence of the quantum correction to the conductivity, at least two characteristic fields should be introduced: B_φ and B_{tr} where

$$B_\varphi = \frac{\hbar}{4eD\tau_\phi}, \quad B_{tr} = \frac{\hbar}{4eD\tau}. \qquad (2)$$

Here $D=l^2/2\tau$ is the diffusion coefficient, $l=v_F\tau$ is the mean-free path, v_F is the Fermi velocity while τ and τ_φ are the transport time and the phase-breaking time, respectively. Assuming two-dimensional electrons with a parabolic band (as we will argue below), B_{tr} can be calculated from the concentration and mobility values. On terraces we expect $B_{tr}\approx 50$ mT while, for steps, $B_{tr}\approx 5$ T. Since, in the first approximation, B_{tr} gives the overall width of the localization peak, this is a clear confirmation that the experimental WL peak is due to the terraces and not to the stripes. To get better values, we performed a fit of the magnetoconductance of terrace using the formula,[12]

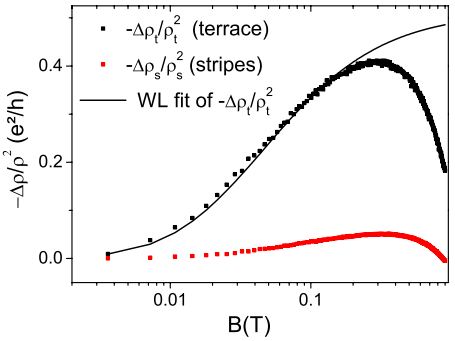

FIG. 5. (Color online) (a) Variations in magnetoconductance for the stripes ($-\Delta\rho_s/\rho_s^2$, red squares) and for the terraces($-\Delta\rho_t/\rho_t^2$, black squares), calculated from the data of Fig. 4(b). The thin black line is a fit of the terrace conductance according to the weak localization formula [see Eq. (3)]. All parameters are given in the text.

$$\frac{\Delta\rho_t}{\rho_t^2} = \frac{e^2}{2\pi^2\hbar}[\Psi(1/2 + B_{tr}/B) - \Psi(1/2 + B_\varphi/B)]. \quad (3)$$

From the best fit shown in Fig. 5, we get $B_\varphi \approx 4$ mT and $B_{tr} \approx 20$ mT corresponding to $\mu_t \approx 2500$ cm^2/V s, in fair agreement with the mobility previously determined for the terraces. On the opposite, the solution we rejected (higher mobility in the stripes) cannot explain the WL peak. In this case, the estimated conductance of the stripes still has a WL-type peak but the width of this peak (if attributed to WL) does not correspond to the high mobility, as expected. Furthermore, the fit using Eq. (3) is very poor.

Here, we restrict ourselves employing the WL-based interpretation of the negative magnetoresistance. However, alternative approaches may be needed. For instance, the temperature dependence of the resistance (even in a moderate magnetic field of ≈ 0.5 T) has still a logarithmic dependence, suggesting the presence of electron-electron interactions.[12] Also, the negative magnetoresistance peak survives up to 30 K, in a temperature range for which the metallic state is well established [with respect to the curve presented in Fig. 4(a)]. It is worth to note that an orbital negative magnetoresistance is also expected[13,14] for doped Mott insulators and may provide an interesting scenario for a negative magnetoresistance peak well above the minimum in $R(T)$.

Before concluding, we demonstrate that quasiparticles we are dealing with are two-dimensional electrons with a parabolic (massive) electron spectrum. To this end, we fitted the SdH oscillations using the Lifshitz-Kosevich[15,16] formula in which only the first harmonic is retained,

$$\delta R_{xx} \propto D_T D_D \cos(j\pi E_F/\hbar\omega_c - \varphi). \quad (4)$$

Here D_D is the Dingle factor: $D_D = \exp(-\pi/\omega_c\tau_e)$, D_T is temperature amplitude factor: $D_T = \gamma/\sinh(\gamma)$ with $\gamma = 2\pi^2 k_B T/\hbar\omega_c$; τ_e is the elastic time, E_F is the Fermi energy, $\omega_c = eB/m_c$ is the cyclotron frequency, m_c is the cyclotron mass, and φ is a phase factor and j an integer. The phase φ determines the nature of the carriers. For a graphene layer: $j=1$ and $\varphi=0$. For two-dimensional massive carriers: $j=2$ and $\varphi=\pi$. For three-dimensional massive carriers, $j=2$ and $\varphi \approx 0.75\pi$. Figure 6(a) shows the evolution of the SdH oscillations at temperatures ranging from 4 to 50 K. In Fig. 6(b), we show that the damping of these oscillations versus T at $B \approx 11.6$ T is well described by the D_T factor with a cyclotron mass $m_c = 0.085\ m_0$ in which m_0 is the free electron mass.

In Fig. 7, we compare the SdH oscillations regime at 4.2 K with the best fit obtained from Eq. (4). The fit yields a phase $\varphi \approx 0.75\pi$. Performing similar analysis for the SdH oscillations in the other Hall bars confirmed that the phase is between $0.75\pi - \pi$ and it does not depend on the Hall-bar orientation. Since this phase value rules out monolayer graphene or turbostratic FLG, for which the expected phase is zero, we imposed $j=2$. We know that the frequency B_f of the SdH oscillations is about $B_f \approx 110$ T and, for a parabolic band with spin and valley degeneracies, this gives a concentration $n_s \approx 2eB_f/\hbar\pi \approx 10^{13}$ cm^{-2}. Once again, this is in excellent agreement with our previous conclusions obtained

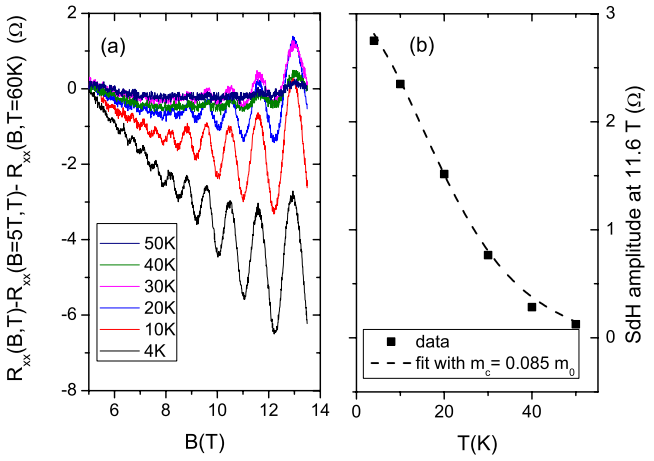

FIG. 6. (Color online) (a) SdH oscillations for various temperatures ranging from 4 to 50 K; (b) SdH amplitude extracted from (a) at $B=11.6$ T (solid square) and best fit (dashed line) according to the Lifshitz-Kosevich formula, using a cyclotron mass $m_c = 0.085 m_0$.

from Hall measurements. The Fermi energy and the elastic time can next be extracted from the data. We find $E_F = 150$ meV and $\tau_e = 40$ fs.[17]

Such combined determinations of φ, E_F, m_c, and n_s, allow to identify how many graphene layers are involved in the conductance mechanism. First, we notice that the cyclotron effective mass is significantly larger than expected for highly oriented pyrolitic graphite (HOPG) graphite,[18] monolayer or bilayer graphene with the density of 10^{13} cm^{-2}. We also notice that any electric field perpendicular to the graphene plane opens a gap, shifts the subbands and (at fixed carrier concentration) increases the cyclotron effective mass ($2\pi m_c = \partial\mathcal{A}/\partial E|_{E=E_F}$ in which $\mathcal{A}$ is the area in k space enclosed by the orbit). Since, on the Si face of SiC, the large

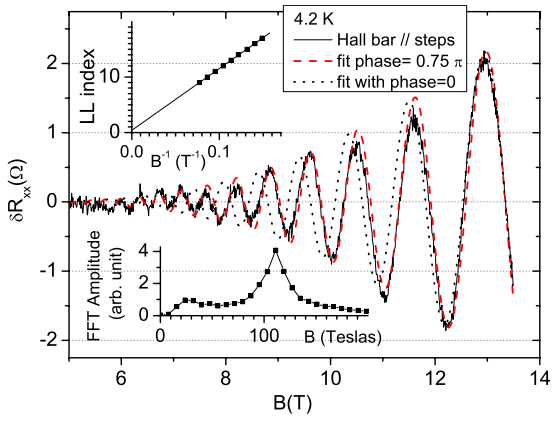

FIG. 7. (Color online) Black line: variations in the longitudinal resistance δR_{xx} obtained for the Hall bar parallel to the step after subtraction of a polynomial background. Red line: best fit according to the Lifshitz-Kosevich formula (see text). The phase was 0.75π and we assumed a cyclotron mass $0.085 m_0$. Dotted dark line: counterexample with phase 0. Upper inset: LL indexes as a function of the position of the SdH maxima. Lower inset: amplitude of the FFT (fast Fourier transform) showing the existence of a maximum at $B=110$ T.

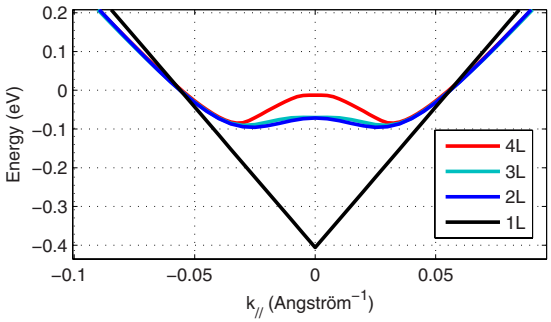

FIG. 8. (Color online) Conduction-band structure of monolayer (black line), bilayer (blue line), trilayer(cyan line), and four-layer graphene (red lines) assuming Bernal stacking. Only the partially occupied bands are shown. The energy reference is E_F. The screening length was taken as $\lambda_s=2$ Å. The effect of trigonal warping was neglected.

electron concentration induced by the buffer layer results in a strong electric field at the SiC/FLG interface (creating conducting surface states[4,19,20]), the finite m_c value is a consequence of this field. To identify the number of participating layers, we plot in Fig. 8 the band structure of monolayer, bilayer, trilayer, and four-layer graphene, assuming a Bernal stacking. Our calculation is based on a tight-binding model[21] which neglects trigonal warping but takes into account the electrochemical potential variations from layer to layer. The latter depends on the interlayer screening length λ_s and, in good agreement with angle-resolved photoemission spectroscopy[19] and scanning tunneling spectroscopy,[4] we take a Fermi velocity $v_F=1.1\times10^6$ cm^{-2} and a screening length $\lambda_s=2$ Å. Using these parameters together with experimental carrier concentration, the conduction bands for 1 to 4 layers have been reconstructed (Fig. 8). For each stacking, the cyclotron mass can be numerically determined and, in this way, we get $m_c/m_0=0.06$ for a monolayer and $m_c/m_0\approx0.08$ for 2, 3, and 4 graphene layers. This is fairly independent of the value chosen for λ_s and, in our case, taking values between 1.4 and 5 Å give similar and reasonable results and conclusions. Every time, for 2 to 4 graphene layers the model reproduces fairly well the cyclotron mass, $n_s(\propto k_F^2/\pi)$ and E_F ($\sim$100 meV, see Fig. 8).

V. CONCLUSION

Raman and magnetoresistance experiments performed on a few-layer graphene samples grown on the Si face of 6*H*-SiC revealed a periodic structure of terraces and stripes, continuously covered by FLG films with an electrical conduction governed by the first (2–4) graphene layers above the buffer layer. The observed in-plane electrical anisotropy originates from the steplike sample morphology that leads to inhomogeneous electron mobility. FLG films are characterized by a Bernal graphene layer stacking and electrons are massive quasiparticles. We attribute a lower electron mobility to the steps edges characterized by a large density of structural defects documented by various research groups. During the preparation of this paper, we became aware on a similar work where the in-plane anisotropy in epitaxial graphene films has been observed and studied electrically.[22]

ACKNOWLEDGMENTS

We acknowledge the EC for partial support through the RTN ManSiC Project, the French ANR for support through the GraphSiC Project, FAPESP, CNPq Brazilian scientific agencies, and INCT NAMITEC. One of us (N.C.) acknowledges the Spanish Government for a Grant Juan de la Cierva 2006. We gratefully acknowledge useful discussions with W. Zawadzki.

[1] P. Sutter, Nat. Mater. **8**, 171 (2009).
[2] T. Seyller *et al.*, Surf. Sci. **600**, 3906 (2006).
[3] T. Shen, J. J. Gu, M. Xu, Y. Q. Wu, M. L. Bolen, M. A. Capano, L. W. Engel, and P. D. Ye, Appl. Phys. Lett. **95**, 172105 (2009).
[4] P. Lauffer, K. V. Emtsev, R. Graupner, T. Seyller, L. Ley, S. A. Reshanov, and H. B. Weber, Phys. Rev. B **77**, 155426 (2008).
[5] F. Varchon *et al.*, Phys. Rev. Lett. **99**, 126805 (2007).
[6] A. Tzalenchuk, S. Lara-Avila, A. Kalaboukhov, S. Paolillo, M. Syvajarvi, R. Yakimova, O. Kazakova, T. J. B. M. Janssen, V. Fal'ko, and S. Kubatkin, Nat. Nanotechnol. **5**, 186 (2010).
[7] N. Camara, J.-R. Huntzinger, G. Rius, A. Tiberj, N. Mestres, F. Pérez-Murano, P. Godignon, and J. Camassel, Phys. Rev. B **80**, 125410 (2009).
[8] A. C. Ferrari *et al.*, Phys. Rev. Lett. **97**, 187401 (2006).
[9] D. Graf, F. Molitor, K. Ensslin, C. Stampfer, A. Jungen, C. Hierold, and L. Wirtz, Nano Lett. **7**, 238 (2007).
[10] C. Faugeras, A. Nerriere, M. Potemski, A. Mahmood, E. Dujardin, C. Berger, and W. A. de Heer, Appl. Phys. Lett. **92**, 011914 (2008).
[11] M. Sprinkle J. Hicks, A. Tejeda, A. Taleb-Ibrahimi, P. Fevre, F. Bertran, H. Tinkey, M. Clark, P. Soukiassian, D. Martinotti, J. Hass, W. De Heer, C. Berger, and E. Conrad, arXiv:1001.3869 (unpublished).
[12] G. Bergmann, Phys. Rep. **107**, 1 (1984).
[13] L. B. Ioffe and P. Wiegmann, Phys. Rev. B **45**, 519 (1992).
[14] J. E. Drut and T. A. Lähde, Phys. Rev. B **79**, 165425 (2009).
[15] I. M. Lifshitz and A. M. Kosevich, Sov. Phys. JETP **2**, 636 (1956).
[16] V. P. Gusynin and S. G. Sharapov, Phys. Rev. B **71**, 125124 (2005).
[17] The elastic time is comparable with the transport time τ_{tr} deduced from the mobility $\tau_{tr}=m_c\mu_s/eV\approx70$ ps; $\tau_{tr}\sim\tau_e$ suggests that short range scattering is dominant, see M. Monteverde, C. Ojeda-Aristizabal, R. Weil, K. Bennaceur, M. Ferrier, S. Guéron, C. Glattli, H. Bouchiat, J. N. Fuchs, and D. L. Maslov, Phys. Rev. Lett. **104**, 126801 (2010); E. H. Hwang and S. Das Sarma, Phys. Rev. B **77**, 195412 (2008).
[18] N. B. Brandt, S. M. Chudinov, and Y. G. Ponomarev, *Semimetals 1. Graphite and its Compounds* (North-Holland, Amsterdam, 1988).

[19] T. Ohta, A. Bostwick, J. L. McChesney, T. Seyller, K. Horn, and E. Rotenberg, Phys. Rev. Lett. **98**, 206802 (2007).

[20] K. S. Novoselov, A. K. Geim, S. V. Morozov, D. Jiang, Y. Zhang, S. V. Dubonos, I. V. Grigorieva, and A. A. Firsov, Science **306**, 666 (2004).

[21] A. H. Castro Neto, F. Guinea, N. M. R. Peres, K. S. Novoselov, and A. K. Geim, Rev. Mod. Phys. **81**, 109 (2009).

[22] M. K. Yakes, D. Gunlycke, J. L. Tedesco, P. M. Campbell, R. L. Myers-Ward, C. R. Eddy, Jr., D. Kurt Gaskill, P. E. Sheehan, and A. R. Laracuente, Nano Lett. **10**, 1559 (2010).